

Article

Room-Temperature NO₂ Gas Sensors Based on Granulated Carbon Nanofiber Material

Alexander G. Bannov^{1,*}, Nikita I. Lapekin¹, Pavel B. Kurmashov¹, Arina V. Ukhina² and Anton Manakhov^{3,4,*}

¹ Department of Chemistry and Chemical Engineering, Novosibirsk State Technical University, 630073 Novosibirsk, Russia

² Institute of Solid State Chemistry and Mechanochemistry SB RAS, Kutateladze 18, 630090 Novosibirsk, Russia

³ National University of Science and Technology "MISIS", Leninsky Prospekt 4, 119049 Moscow, Russia

⁴ Research Institute of Clinical and Experimental Lymphology—Branch of the ICG SB RAS, 2 Timakova St., 630060 Novosibirsk, Russia

* Correspondence: bannov.alexander@gmail.com (A.G.B.); manakhov@mail.muni.cz (A.M.)

Abstract: Room-temperature gas sensors based on granulated carbon nanofiber material were investigated for the detection of NO₂. The granulated material consisting of intertwined carbon nanofibers was synthesized by the decomposition of CH₄ over the Ni/Al₂O₃ catalyst in a vibro-fluidized bed reactor. Carbon material was investigated using transmission electron microscopy, Raman spectroscopy, low-temperature nitrogen adsorption, and X-ray photoelectron spectroscopy. Investigation of the gas sensors towards NO₂ at room temperature (25 ± 2 °C) was carried out in a dynamic flow-through setup in the range from 1 to 500 ppm. A comparison of the sensitivity gas sensor to NH₃ and CH₄ was also given. The sensor based on non-treated carbon nanofiber material showed the response ΔR/R₀ of 5.1 % to 10 ppm of NO₂. It was found that the sensor response to NO₂ decreased when increasing the relative humidity. The effect of the relative humidity was more pronounced for low concentrations of nitrogen dioxide and decreases with a further increase in them.

Keywords: carbon nanofibers; carbon nanomaterials; sensors; gas sensors; nitrogen dioxide; response; humidity; ammonia



Citation: Bannov, A.G.; Lapekin, N.I.; Kurmashov, P.B.; Ukhina, A.V.; Manakhov, A. Room-Temperature NO₂ Gas Sensors Based on Granulated Carbon Nanofiber Material. *Chemosensors* **2022**, *10*, 525. <https://doi.org/10.3390/chemosensors10120525>

Academic Editor: Manuel Alexandre

Received: 20 October 2022

Accepted: 7 December 2022

Published: 10 December 2022

Publisher's Note: MDPI stays neutral with regard to jurisdictional claims in published maps and institutional affiliations.



Copyright: © 2022 by the authors. Licensee MDPI, Basel, Switzerland. This article is an open access article distributed under the terms and conditions of the Creative Commons Attribution (CC BY) license (<https://creativecommons.org/licenses/by/4.0/>).

1. Introduction

Detection of hazardous gases is an important problem in the fields of environmental protection, and the chemical and food industry. One of these gases is nitrogen dioxide (NO₂), which is a widely used compound in the manufacturing of explosives, nitric acid, etc. Determination of low concentrations of NO₂ is of interest in order to carry out the monitoring of the environment. The impact of this gas on human beings can cause various injuries (depending on concentration) such as edema, irritation effect to nose and throat, cough, etc. Now, the problem of the creation of room-temperature gas sensors for detection of hazardous gases is extremely important [1–4]. The application of various nanomaterials makes it possible to operate the gas sensors at a considerably lower temperature (even at room temperature) compared to conventional semiconductor-based sensors (i.e., above 300–350 °C) [5–7]. The possibility to create the room-temperature sensors will make it possible to integrate them in mobile devices, since these devices will possess a lower consumption of energy. The urgent problems of the NO₂ gas sensors are high performance, low-power consumption and low cost [8] which can be solved by the use of proper high-quality sensing material.

There are many nanomaterials and composites used for the creation of room-temperature NO₂ gas sensors, such as Fe₂O₃ [9], MoS₂/SnO₂ [10], MoS₂/reduced graphene oxide [11], C₃N₄@TiO₂ [12], MoS₂/Ti₃C₂T_x MXene [13], α-MoO₃ [14] etc. Photoactivated materials are also used for the detection of NO₂ [15]. Much attention has been paid to the application of

carbon nanomaterials for nitrogen dioxide sensing, such as multi-walled carbon nanotubes (MWCNTs) [16], single-walled carbon nanotubes (SWCNTs) [17–19], graphene oxide [20], reduced graphene oxide [21], graphene [22], carbon nanofibers [23,24], and their hybrids or composites [25]. However, all these materials are hard to produce, especially composites and hybrids, which is inconvenient for the scale-up of sensors manufacturing. Sensing materials can be applied either in the form of films [26] or pellets (compacted powder) [27].

Usually, the carbon nanofibers (CNFs) are synthesized in the form of a powder formed by the growth of carbon on the catalysts with relatively low content of active components (e.g., Ni, Ni-Cu) [28,29]. The use of a catalyst with high content of active components makes it possible to obtain not a powder, but granules [30–32]. This material can be used for the synthesis of refractory compounds [33–35], as a filler for conductive epoxy composites [36], such as electrode for supercapacitors [37], and catalyst for the selective oxidation of H₂S to sulfur [32,38] etc. Since the synthesis method of CNFs is an attractive CO_x-free process [29,39,40] that may be applied to produce both hydrogen and carbon nanomaterials, the important task is to find the application of latter. One of the novel applications of the granulated CNF material for gas sensors was not yet investigated. The low cost and high yield of the CNFs' formation over high-percentage nickel-containing catalysts are high enough compared to MWCNTs and SWCNTs, and determine no significant need in the purification of a sample creating the advantage of CVD CO_x-free catalytic decomposition of methane and C₁-C₄ hydrocarbons for further scale-up [41,42]. Therefore, it is important to study the possibility to create the films for detection of NO₂ at room temperature, which are based on the granulated CNF material. This type of active material will make the sensor cheaper and will be produced using an important CO_x-free process as a by-product of turquoise hydrogen production [43,44]. Therefore, this type of material can be considered as more convenient for sensing applications, and it has not been previously investigated in this field.

This work was devoted to the creation of a room temperature NO₂ gas sensor based on CNFs that were grown on the Ni/Al₂O₃ catalyst with high content of the active component. The composition of the catalyst made it possible to obtain the granulated materials consisting of intertwined carbon nanofibers. The paper is devoted to the application of initial, i.e., non-treated CNF material. The response of the CNF-based sensor was investigated in a range of nitrogen dioxide concentrations 1–500 ppm. The effect of the relative humidity (RH) on the sensing behavior of the CNFs was also analyzed.

2. Materials and Methods

2.1. Synthesis and Characterization of CNFs

The granulated CNF material was synthesized by the decomposition of methane in a flow vibrofluidized bed reactor [45] over 90% Ni/10% Al₂O₃ catalyst. The catalyst was obtained by the coprecipitation technique. The decomposition of methane was carried out at 550 °C (flow rate was 550 L/h).

The yield of CNFs during synthesis was 100 g/g_{cat}. The carbon material consisted of granules 1–5 mm in diameter. The granules were formed as a result of the growth of material on the catalytic nanoparticles with high content of active components (i.e., nickel). The methods described below were used for the characterization of the carbon material synthesized.

Transmission electron microscopy (TEM) was carried out using JEM-2010 microscope (JEOL, Tokyo, Japan) at the accelerating voltage of 80–200 kV. X-ray diffraction of CNFs was carried out using DRON-3 diffractometer (Cu K α radiation, 1.54 Å). Defectiveness of CNFs was studied using the Raman spectroscopy instrument T64000 Horiba Jobin Yvon ($\lambda = 514$ nm). Low-temperature nitrogen adsorption method was used for the determination of the specific surface area using the Nova Quantachrome 1200 e installation. The chemical composition of carbon nanomaterial was determined by X-ray photoelectron spectroscopy (XPS) using the electron spectrometer SPECS (SPECS Surface Nano Analysis GmbH, Berlin, Germany) (Al K α , $h^* = 1486.74$ eV).

2.2. Creation of Sensor and Investigation

The sensors were created by the drop-casting technique. The CNFs were deposited on the textolite substrate (10×10 mm) with copper electrodes (Figure 1a). The area of deposition of the active layer was 8×8 mm. The dispersion of the CNFs (particles were ground in a mortar and preliminary sieved through a sieve with 100- μ m mesh size) was created by sonication (22 kHz, ultrasonic bath UZV-3/200 RELTEC, Yekaterinburg, Russia). The sonication was carried out in a volume of ethanol (5 mL of solvent per 0.03 g of CNFs) for 20 min (power was 85 W). The droplets were deposited on the substrate heated to 80 °C and formed the active layer, covering the copper electrodes.

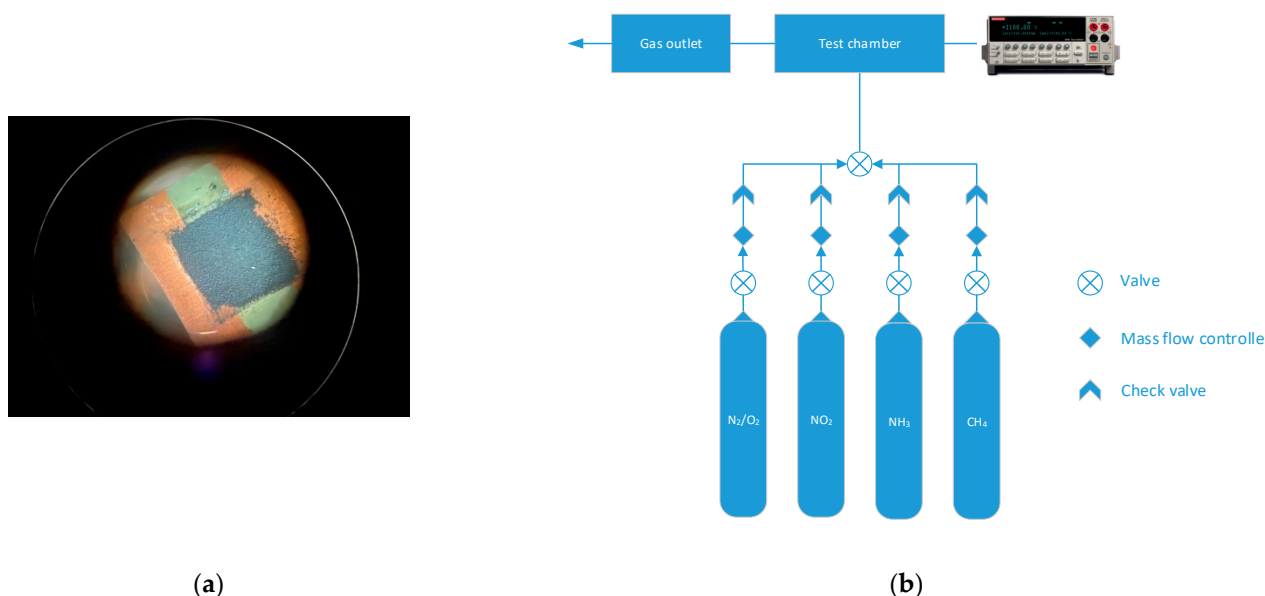


Figure 1. Photo of the active material (namely CNFs) on the copper electrodes on the textolite substrate (a); scheme of the installation for sensor testing (b).

The gas sensor was investigated using the custom-built setup (Figure 1b).

The measurements were carried out with two gas channels: synthetic air (79 vol% N₂, 21 vol% O₂) and the analyte (NO₂, NH₃, CH₄ diluted in synthetic air with the concentration of analyte 5000 ppm). Three different gases were used for the testing of the sensors in order to check the selectivity of the sensors. Additionally, two gases with different natures of interaction with carbons were used, e.g., NO₂ is an electron acceptor, and NH₃ is electron donating compound.

The scheme of the setup is described in [27] in detail. The sensor was placed on the ceramic plate (heater). The resistance of the layer of the CNF material was measured using a two-point technique between the copper electrodes by Keithley 2401 Source Meter (Keithley, Cleveland, OH, USA). Data acquisition was made by KickStart software (Tektronix, Beaverton, OR, USA). The bias voltage was 0.1 V. The sensor response was calculated using the following equation:

$$\Delta R/R_0 = ((R - R_0)/R_0) \times 100\%, \quad (1)$$

where R and R_0 were the sensor resistances in the mixture of analyte + synthetic air and pure synthetic air, respectively (Ω). The concentration of NO₂ as the main gas investigated for testing of the sensor was varied from 1 ppm to 500 ppm. The temperature of measurements was 25 ± 2 °C. The relative humidity (RH denoted as φ) of air was controlled by the flow of air passing through a bubbler and can be ranged from 10 to 70%. Temperature and related humidity inside the chamber were measured by the corresponding sensors.

There are three main characteristics analyzed in this paper, such as sensor response, response time, and recovery time. An additional characteristic was the sensitivity deter-

mined as a slope of dependence of response on the concentration calculated on the basis of the linear fitting of the experimental data.

3. Results and Discussion

3.1. Investigation of Granulated CNF Material

The sample consisted of carbon nanofibers 40–80 nm in diameter (Figure 2). The CNFs were strongly curved. There are nanoparticles of the catalyst covered by the carbon shell. The sample was mainly represented by fish-bone structure carbon nanofibers.

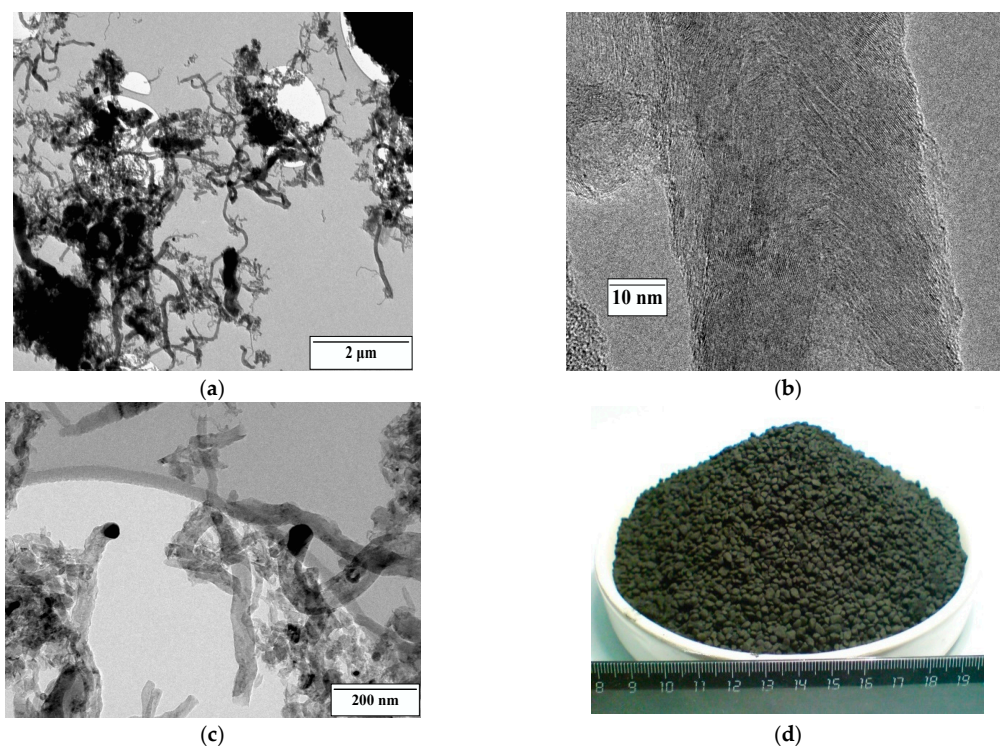


Figure 2. TEM images of carbon nanofibers used as an active material for gas sensors (a–c) and the photo of as-received granules of CNF material (d).

XRD pattern is shown in Figure 3. It was shown that the sample is fully represented by carbon material. The phases of Ni or Al_2O_3 are absent confirming their low content in the material. The interlayer spacing d_{002} was 3.42 Å which is far from pure graphite and typical for disordered carbon materials. Crystallite width L_c calculated using the Sherrer equation was 84 Å [46].

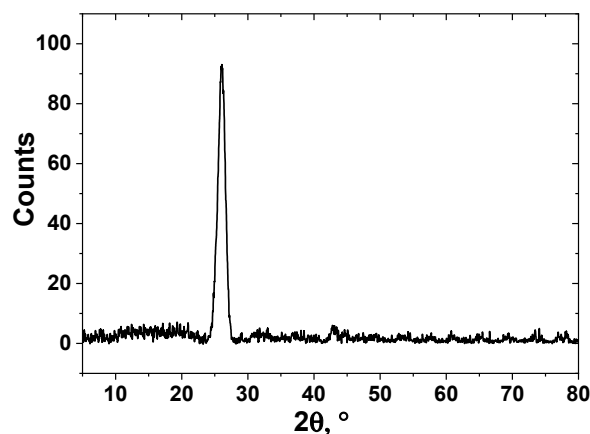


Figure 3. XRD pattern of CNF sample (Cu $K\alpha$ radiation, $\lambda = 1.54$ Å).

The Raman spectrum of the carbon nanomaterial is shown in Figure 4a. There were three main peaks presented, D (1344 cm^{-1}), G (1569 cm^{-1}), and the small shoulder of D' (1600 cm^{-1}) peak. The defectiveness of the CNFs is high enough ($I(D)/I(G) = 0.98$) and somehow correlates with other carbon nanomaterials. The crystallite width calculated using the Tuinstra–Koenig Equation (2) showed $L_a = 4.5\text{ nm}$ [47].

$$L_a = C \times (I(D)/I(G)), \quad (2)$$

where $C = 4.4\text{ nm}$.

According to low-temperature nitrogen adsorption, the specific surface area of the sample was $110\text{ m}^2/\text{g}$ (fully mesoporous material), which is typical for fish bone structure materials [48].

According to XPS, there is no nickel detected in the material (Figure 4b). This fact indicates that the nanoparticles were completely covered by a carbon shell and there is no direct contact between the gas phase (e.g., air) and nickel nanoparticles. The O/C ratio was 0.033, indicating a relatively low concentration of oxygen-containing groups on the surface of the CNFs, taking into account that the sample was not subjected to any treatment.

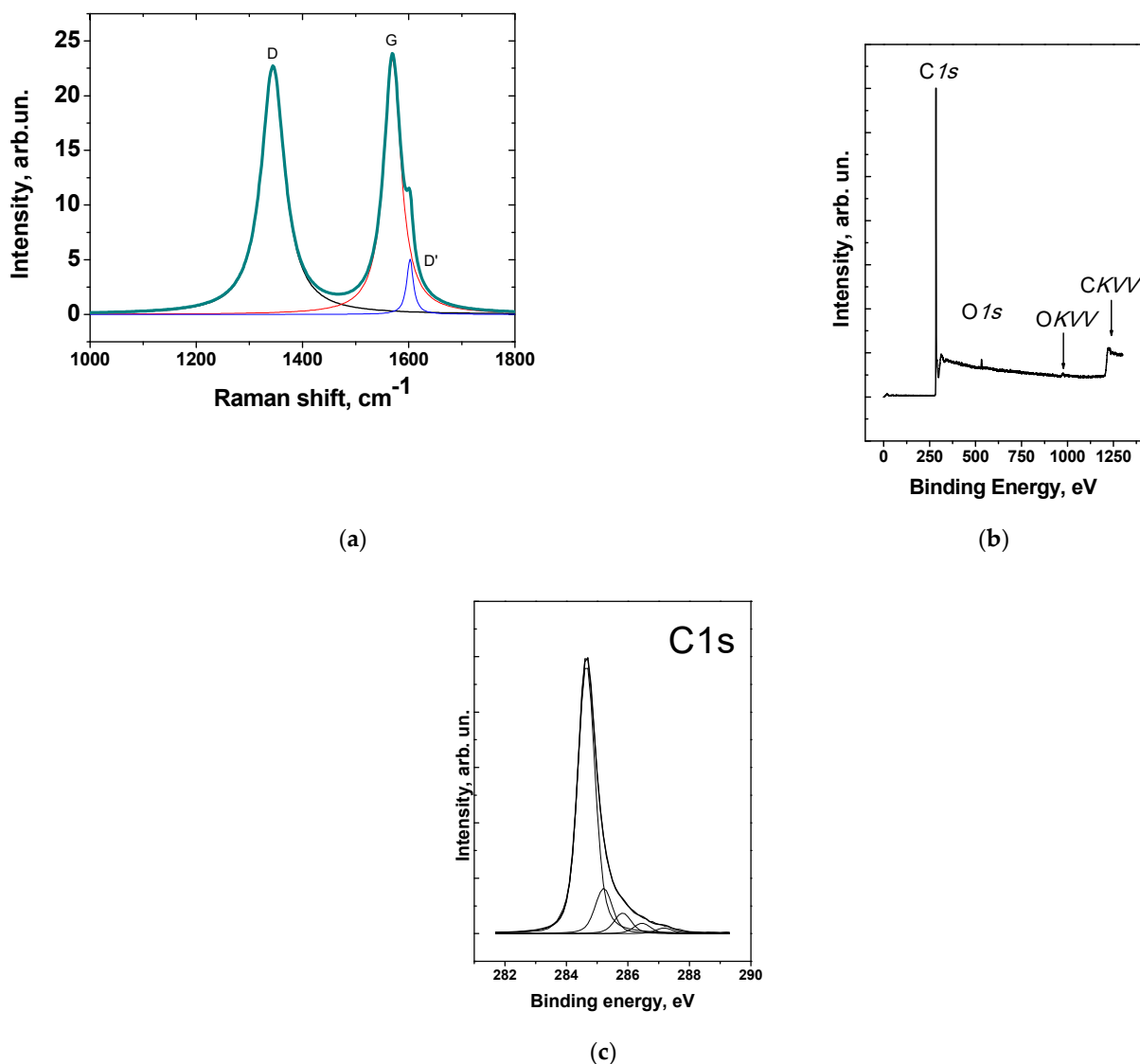


Figure 4. Raman spectrum ($\lambda = 514\text{ nm}$) (a); survey XPS spectrum (b); C1s spectrum of CNF material (c) Reproduced with permission of Elsevier [49].

3.2. Testing of Gas Sensor

The contact with NO₂ induced a decrease in sensor resistance (Figure 5). The response of the sensor ranged from 0.86% (1 ppm NO₂) to 16% (50 ppm NO₂). The drop in resistance upon contact with nitrogen dioxide is a result of an increase in the concentration of charge carriers during the adsorption of the compound. Initially, the resistance of the sensor active layer was 409 Ω, indicating good conducting properties of the CNFs, compared to other materials, such as graphene oxide, reduced graphene oxide, etc. [27,50]. Taking into account the sensing curves, it is worth noting that there is an incomplete recovery of the sensor. This phenomenon can be related to the incomplete desorption of NO₂ from the surface of the CNFs. Although researchers typically related the dominating mechanism of the nitrogen dioxide interaction with the surface of the carbons to be physical adsorption [51,52], in fact, for the CNFs studied the chemisorption also takes place, leading to an incomplete recovery. However, physical adsorption dominates obviously.

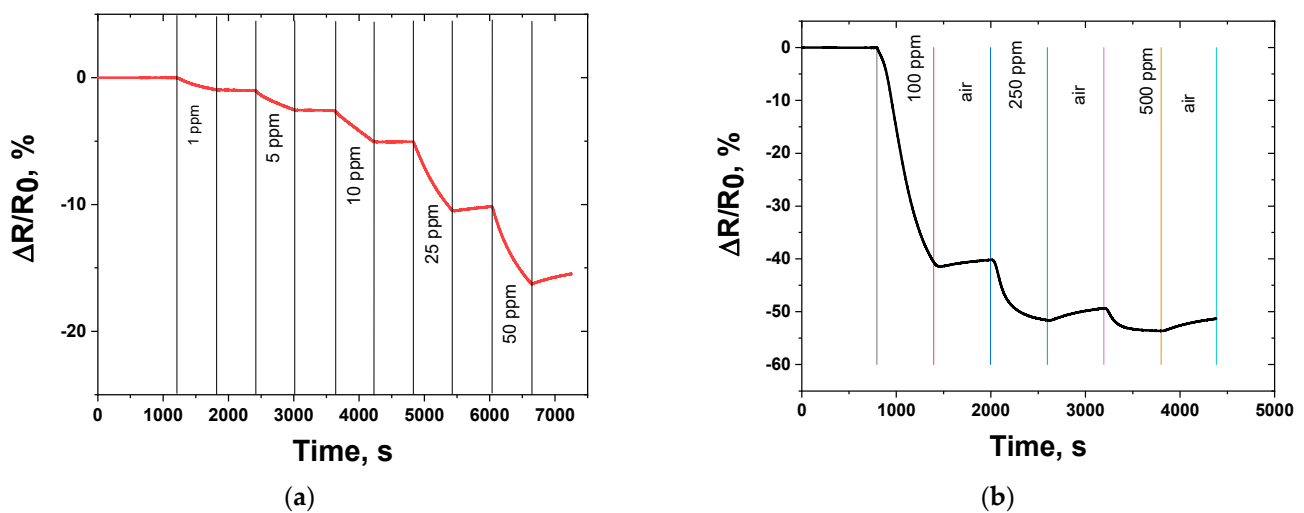


Figure 5. Comparison of the response of sensors based on granulated CNF material to NO₂ at room temperature (25 ± 2 °C, air) in different ranges: (a) 1–50 ppm; (b) 100–500 ppm.

The results of the effect of the RH on the sensor response are presented in Table 1. It was shown that the increase of the RH induced a decrease in $\Delta R/R_0$ and the drop of response was stronger at lower concentrations (i.e., 100 ppm). Further increase of the RH to 60% and 70% showed the response of 9.1% and 8.6%, respectively (at 100 ppm), showing the weakening role of the RH impact.

Table 1. Effect of relative humidity of air on the response of sensors based on granulated CNF material at room temperature (25 ± 2 °C, air) to NO₂ and NH₃.

Relative Humidity φ , %	$\Delta R/R_0$ at Various NO ₂ Concentration, %			$\Delta R/R_0$ at Various NH ₃ Concentration, %		
	100 ppm	250 ppm	500 ppm	100 ppm	250 ppm	500 ppm
20	41.4	51.6	53.6	6.3	18	24.9
40	12.4	28.7	31.2	n/a	3	6.6
60	9.1	21.9	26.8	0.3	1.29	3.8
70	8.6	14.4	19.9	n/a *	n/a	n/a

* The noise interfered to obtain the data.

In general, the dependence of the sensor response of NO₂ on the RH can be described by the power law of the type $y = a \times x^b$: $\Delta R/R_0 = 3322.95951 \times \varphi^{-1.46687}$ ($R^2 = 0.98498$) at 100 ppm; $\Delta R/R_0 = 728.80867 \times \varphi^{-0.88231}$ ($R^2 = 0.98318$) at 250 ppm; $\Delta R/R_0 = 467.60219 \times \varphi^{-0.72406}$ ($R^2 = 0.98223$) at 500 ppm. From this, it follows that the effect of humidity is

more pronounced for low concentrations of nitrogen dioxide and decreases with a further increase in them. Usually, the increase in RH induced the rise of response, for example, this effect was reported for the WS₂/graphene aerogel sensor [53] and the graphene FET sensor [54]. The authors supposed that humidity acts as an acceptor [54]. Usually, in these articles, the increase in the NO₂ sensor when increasing the RH is related to the donation of protons H⁺ of H₃O⁺ (from H₂O) to the material. But the data obtained for the granulated CNF material at room temperature showed the opposite relations. Probably, such an effect can be caused by the occupation of absorption sites with water molecules as a result of the rise of the RH, which prevents the adsorption of NO₂ molecules.

A comparison of sensing behavior was also carried out for NH₃ detection at room temperature. Detection of ammonia was taken in order to compare the behavior of CNFs under the adsorption of different types of gas, since the latter is an electron-donating compound. The sensor response to NH₃ was more than two times lower compared to NO₂ (Table 1). The increase in the RH of the air induced the drop of $\Delta R/R_0$ more than 4–5 times depending on the concentration. However, the increase in the RH from 60% to 70% induced the increase in response, which is caused by the beginning of the dissolution of ammonia in the film of water absorbed on the surface of the carbon nanofibers [55].

For ammonia, similar dependences were found, when the response of the sensor $\Delta R/R_0$ decreased with an increase in the RH of the air. This is typical for materials that have not been functionalized or contain a small number of functional groups themselves (according to the XPS data, the oxygen content was 3.3 at.%; sample CNF-1 investigated in [49]). The decomposition of the C1s spectrum showed five peaks at 284.65 eV (76.7%), 285.21 (12.9%), 285.83 eV (5.9%), 286.46 eV (2.9%), 287.2 eV (1.6%) related to the C–C sp²-hybridized carbon atoms, the carbon atoms in the sp³ hybridization, and the carbon atoms which are chemically bonded to oxygen (COC, COH, and C=O groups), respectively. At the same time, for the highly oxidized carbon materials, such as graphite oxide, an increase in the RH of the air, on the contrary, causes an increase in the relative response of the sensor [55,56]. The response in relatively dry air (e.g., RH 20%) can be considered high enough and comparable with some pristine carbon nanotube-based sensors [50] or plasma-functionalized carbon nanomaterials [57].

The use of the third model gas (CH₄) did not show any significant response of the sensor (the relative response was comparable to the level of noise of the resistance measured) (Figure 6a).

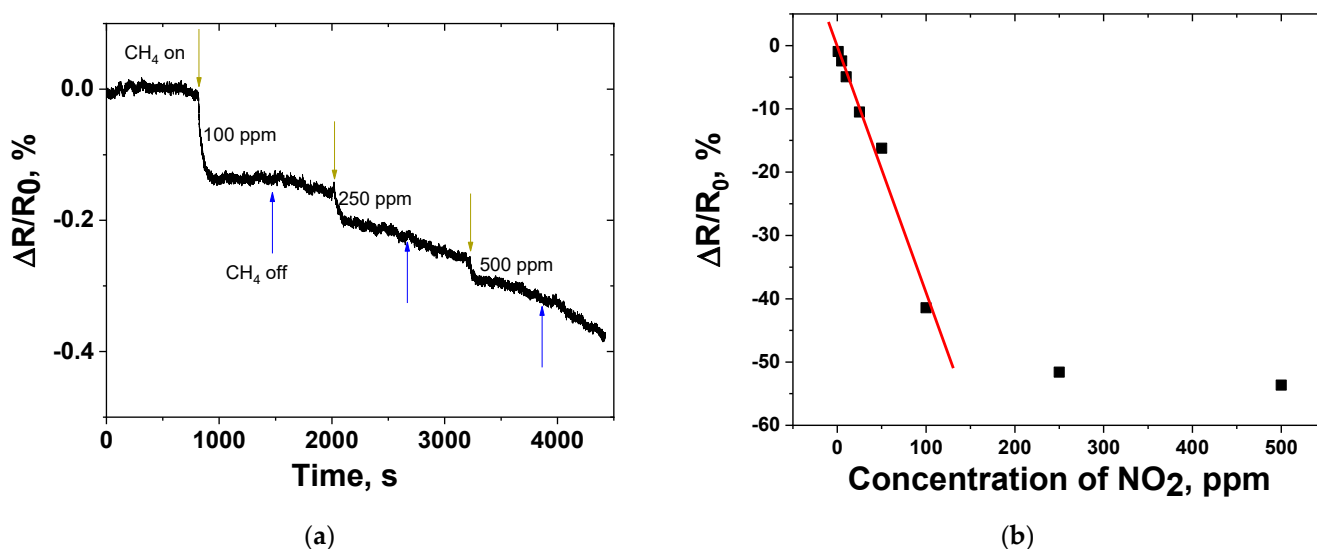


Figure 6. (a) Response of CNF-based gas sensor to CH₄ at room temperature (25 ± 2 °C, air); (b) Response vs. concentration of NO₂ at room temperature. The linear fitting line ($\Delta R/R_0 = -0.39654 \times C_{NO_2} - 0.12341$) is marked with red color.

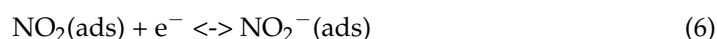
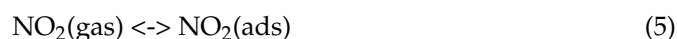
The sensitivity obtained using the linear fitting of the response dependence on the concentration showed that the range of nitrogen dioxide concentrations ($C_{\text{NO}_2} = 1\text{--}100$ ppm) can be treated using a linear function ($\Delta R/R_0 = -0.39654 \times C_{\text{NO}_2} - 0.12341$, $R^2 = 0.9844$); the sensitivity was -0.39654 %/ppm. The saturation appears when the concentration of NO_2 grows above 100 ppm, showing a decrease in the rate of sensor response growth when increasing the concentration (Figure 6b).

3.3. Mechanism of NO_2 Detection and Analysis of Adsorption

The typical mechanism of the resistance change of CNFs is based on the adsorption of oxygen on the surface carbon material [58]. The oxygen ionizes to O_2^- [59]:



The extraction of the charge carriers induces the growth of conductivity of the material during the adsorption of gas [60].



Of course, the pristine material contains a nickel catalyst, but it is covered with a carbon shell (since no Ni was detected according to XPS) and takes part in the transport of electrons only indirectly. Low concentrations of oxygen-containing functional groups (ether, alcohol, and ketone groups' concentrations) were 5.9 at.%, 2.9 at.%, and 1.6 at.% in C1s photoelectron spectra [49]. However, there are different approaches to describe the mechanism of NO_2 adsorption on the surface of carbons. In [61], it was reported that NO (this molecule was a result of the following reaction $2\text{NO}_2 \leftrightarrow \text{NO} + \text{NO}_3$ passing on the surface of nanotubes) and NO_2 are weakly bonded on the surface of the single-walled carbon nanotubes. The results of the calculations showed the high energy of NO_3 molecule adsorption on their surface. The latter effect explained the long recovery of NO_2 during the sensing experiments.

The results of the sensor response were treated on the basis of various isotherms (Table 2). During the fitting, it was supposed that the ratio of a number of adsorption centers occupied as a result of the sorption Q is proportional to the sensor response $\Delta R/R_0$. The best fitting of the response values was achieved for the Modified non-linear Langmuir equation [62]. The energy of adsorption was calculated based on two equations that are both used for the calculation of entropy (Equation (7) [63] and Equation (8) [64]).

$$\Delta S = R \times \ln(R \times T) \quad (7)$$

$$\Delta S = R \times \ln(K) \quad (8)$$

Enthalpy was calculated according to the equation below:

$$\Delta H = -RT \left(\ln(K) + \frac{\Delta S}{R} \right) \quad (9)$$

The enthalpy of adsorption ΔH_{ads} possesses relatively low values indicating the physical character of the NO_2 adsorption on the surface of the granulated CNF material. According to the Table 2, the energy of adsorption determined for the modified non-linear Langmuir equation was 0.111 eV (Equation (7)) and 0.18 eV (Equation (8)).

Table 2. Granulated CNF-based NO₂ gas sensor performance compared to the literature data related to different sensor materials.

Isotherm	Equation	Type of Dependence	R ²	Q _m	K _L (for Langmuir) or K _f (for Freundlich), Pa ⁻¹	n	ΔH _{ads} , eV
Non-linear Langmuir [63,65–68]	$Q = \frac{K_L \times p}{1 + K_L \times p}$	Q vs. p	0.96	68.99	0.1	n/a	0.142 Equation (7)
							0.118 Equation (8)
Modified non-linear Langmuir [62]	$Q = \frac{K_L \times p^n}{1 + K_L \times p^n}$	Q vs. p	0.98	55.85	0.03	1.87	0.111 Equation (7)
							0.18 Equation (8)
Linear Langmuir [65,67,68]	$\frac{p}{Q_m} + \frac{1}{K_L \times Q_m}$	p/Q vs. p	0.96	67.65	0.09	n/a	0.139 Equation (7)
							0.124 Equation (8)
	$\frac{1}{Q_m} + \frac{1}{K_L \times Q_m \times p}$	1/Q vs. 1/p	0.97	17.84	0.05	n/a	0.124 Equation (7)
							0.154 Equation (8)
	$Q_m - \frac{Q}{K_L \times p}$	Q vs. Q/p	0.58	51.82	0.15	n/a	0.152 Equation (7)
0.097 Equation (8)							
$\frac{Q}{p} = K_L \times \frac{1}{Q_m - K_L \times Q}$	Q/p vs. Q	0.58	72.87	0.09	n/a	0.139 Equation (7)	
						0.124 Equation (8)	
Freundlich [65,67–69]	$Q = K_f \times p^n$	Q vs. p	90	-	9.87	0.46	0.259 Equation (7)
							0.118 Equation (8)

Q is the number of adsorption centers occupied as a result of sorption, Q_m is the maximum number of centers occupied, p is the partial pressure of the gas (i.e., NO₂) in air, Pa; ΔH_{ads}—enthalpy of adsorption, eV.

A comparison of data of the response of the CNF-based NO₂ sensor to the literature data is presented in Table 3. The obtained results showed the efficiency of this material for the room-temperature gas sensors, taking into account that there is a pristine material used for the detection of nitrogen dioxide and there were no treatments used to enhance its sensitivity. Taking into account the response of the sensor and the technology of the production of CNFs from C₁–C₄ hydrocarbons coming from associated petroleum gas [39,41,70], the obtained material will be cheap compared to other carbon nanomaterials, such as carbon nanotubes, graphene, reduced graphene oxide, etc., which are relatively expensive.

Table 3. Granulated CNF-based NO₂ gas sensor performance compared to the literature data related to different sensor materials.

Active Material of NO ₂ Sensor	NO ₂ Concentration	Sensor Response	RH	Temperature	Ref.
Polypyrrole	100 ppm	36%	n/a	n/a (room temperature)	[71]
Ozone treated graphene	200 ppm	17%	n/a	n/a (room temperature)	[72]
Fluorinated graphene (CF _{0.33})	100 ppm	32% (in Ar)	n/a	30 °C	[73]
Reduced fluorinated graphite	100 ppm	11% (in Ar)	n/a	n/a (room temperature)	[74]
rGO/AuNP	50 ppm	3.2%	n/a	150 °C	[75]
N-MWCNT	9 ppm	0.16%	n/a	25 °C	[76]
CNFs	10 ppm	5.1%	20%	25 ± 2 °C	This work

4. Conclusions

The presented results demonstrate the efficiency of non-treated granulated carbon nanofiber material as an active material for nitrogen dioxide detection. The sensor based on the non-treated carbon nanofiber material showed the response 5.1% to 10 ppm of NO₂. The data presented confirm the domination of the physical adsorption mechanism of the interaction of NO₂ and carbon nanofibers. Although the concentration of the functional groups in the carbon nanofiber material is low enough, its response is high as for the non-treated material. It was found that the increase in the relative humidity led to a decrease in the sensor response. The CNFs obtained by catalytic decomposition of methane can make the sensor cheaper and can be produced using a CO_x-free process as a by-product of the production of so-called turquoise hydrogen.

Author Contributions: Conceptualization, N.I.L., P.B.K. and A.G.B.; investigation, N.I.L., A.V.U. and A.M.; resources, N.I.L. and A.M.; writing—original draft preparation, N.I.L. and A.G.B. All authors have read and agreed to the published version of the manuscript.

Funding: The work was financially supported as part of the implementation of the NSTU Development program (scientific project No. S22-11).

Institutional Review Board Statement: Not applicable.

Informed Consent Statement: Not applicable.

Conflicts of Interest: The authors declare no conflict of interest.

References

- Bannov, A.G.; Jašek, O.; Prášek, J.; Buršík, J.; Zajíčková, L. Enhanced ammonia adsorption on directly deposited nanofibrous carbon films. *J. Sens.* **2018**, *2018*, 7497619. [[CrossRef](#)]
- Bannov, A.G.; Popov, M.V.; Brester, A.E.; Kurmashov, P.B. Recent Advances in Ammonia Gas Sensors Based on Carbon Nanomaterials. *Micromachines* **2021**, *12*, 186. [[CrossRef](#)] [[PubMed](#)]
- Kumar, R.; Kumar, A.; Singh, R.; Kashyap, R.; Kumar, R.; Kumar, D.; Sharma, S.K.; Kumar, M. Room temperature ammonia gas sensor using Meta Toluic acid functionalized graphene oxide. *Mater. Chem. Phys.* **2020**, *240*, 121922. [[CrossRef](#)]
- Qin, C.; Wang, B.; Wu, N.; Han, C.; Wang, Y. General Strategy to Fabricate Porous Co-Based Bimetallic Metal Oxide Nanosheets for High-Performance CO Sensing. *ACS Appl. Mater. Interfaces* **2021**, *13*, 26318–26329. [[CrossRef](#)] [[PubMed](#)]
- Al-Hashem, M.; Akbar, S.; Morris, P. Role of Oxygen Vacancies in Nanostructured Metal-Oxide Gas Sensors: A Review. *Sens. Actuators B Chem.* **2019**, *301*, 126845. [[CrossRef](#)]
- Lin, T.; Lv, X.; Hu, Z.; Xu, A.; Feng, C. Semiconductor Metal Oxides as Chemoresistive Sensors for Detecting Volatile Organic Compounds. *Sensors* **2019**, *19*, 233. [[CrossRef](#)]

7. Zhang, C.; Liu, G.; Geng, X.; Wu, K.; Debliquy, M. Metal oxide semiconductors with highly concentrated oxygen vacancies for gas sensing materials: A review. *Sens. Actuators A Phys.* **2020**, *309*, 112026. [[CrossRef](#)]
8. Zhang, C.; Luo, Y.; Xu, J.; Debliquy, M. Room temperature conductive type metal oxide semiconductor gas sensors for NO₂ detection. *Sens. Actuators A Phys.* **2019**, *289*, 118–133. [[CrossRef](#)]
9. Dai, Z.; Lee, C.S.; Tian, Y.; Kim, I.D.; Lee, J.H. Highly reversible switching from P- to N-type NO₂ sensing in a monolayer Fe₂O₃ inverse opal film and the associated P-N transition phase diagram. *J. Mater. Chem. A* **2015**, *3*, 3372–3381. [[CrossRef](#)]
10. Luo, J.; Li, C.; Yang, Q.; Yan, L.; Zhang, B.; Tao, R.; Rauf, S.; Li, H.; Fu, C. Facile Fabrication of MoS₂Nanoflowers/SnO₂ Colloidal Quantum Dots Nanocomposite for Enhanced NO₂Sensing at Room Temperature. *IEEE Sens. J.* **2022**, *22*, 6295–6302. [[CrossRef](#)]
11. Li, W.; Li, H.; Qian, R.; Zhuo, S.; Ju, P.; Chen, Q. CTAB Enhanced Room-Temperature Detection of NO₂ Based on MoS₂-Reduced Graphene Oxide Nanohybrid. *Nanomaterials* **2022**, *12*, 1300. [[CrossRef](#)] [[PubMed](#)]
12. Pasupuleti, K.S.; Reddeppa, M.; Chougule, S.S.; Bak, N.H.; Nam, D.J.; Jung, N.; Cho, H.D.; Kim, S.G.; Kim, M.D. High performance langasite based SAW NO₂ gas sensor using 2D g-C₃N₄@TiO₂ hybrid nanocomposite. *J. Hazard. Mater.* **2022**, *427*, 128174. [[CrossRef](#)] [[PubMed](#)]
13. Yan, H.; Chu, L.; Li, Z.; Sun, C.; Shi, Y.; Ma, J. 2H-MoS₂/Ti₃C₂T_x MXene composites for enhanced NO₂ gas sensing properties at room temperature. *Sens. Actuators Rep.* **2022**, *4*, 100103. [[CrossRef](#)]
14. Li, W.; Xing, K.; Liu, P.; Chuang, C.; Lu, Y.R.; Chan, T.S.; Tesfamichael, T.; Motta, N.; Qi, D.C. Ultrasensitive NO₂ Gas Sensors Based on Layered α-MoO₃ Nanoribbons. *Adv. Mater. Technol.* **2022**, *7*, 1–10. [[CrossRef](#)]
15. Šetka, M.; Claros, M.; Chmela, O.; Vallejos, S. Photoactivated materials and sensors for NO₂ monitoring. *J. Mater. Chem. C* **2021**, *9*, 16804–16827. [[CrossRef](#)]
16. Ma, D.; Su, Y.; Tian, T.; Yin, H.; Huo, T.; Shao, F.; Yang, Z.; Hu, N.; Zhang, Y. Highly Sensitive Room-Temperature NO₂Gas Sensors Based on Three-Dimensional Multiwalled Carbon Nanotube Networks on SiO₂Nanospheres. *ACS Sustain. Chem. Eng.* **2020**, *8*, 13915–13923. [[CrossRef](#)]
17. Sayago, I.; Terrado, E.; Horrillo, M.C.; Aleixandre, M.; Fernández, M.J.; Santos, H.; Maser, W.K.; Benito, A.M.; Martinez, M.T.; Gutiérrez, J.; et al. NO₂ detection with single walled carbon nanotube networks. In Proceedings of the 2007 Spanish Conference on Electron Devices, Madrid, Spain, 31 January–2 February 2007; pp. 189–192. [[CrossRef](#)]
18. Mendes, R.G.; Wr, P.S.; Bachmatiuk, A.; Sun, J.; Gemming, T.; Liu, Z.; Rümeli, M.H.; Wróbel, P.S.; Bachmatiuk, A.; Sun, J.; et al. Carbon nanostructures as a multi-functional platform for sensing applications. *Chemosensors* **2018**, *6*, 60. [[CrossRef](#)]
19. Sacco, L.; Forel, S.; Florea, I.; Cojocar, C.-S. Ultra-sensitive NO₂ gas sensors based on single-wall carbon nanotube field effect transistors: Monitoring from ppm to ppb level. *Carbon N. Y.* **2020**, *157*, 631–639. [[CrossRef](#)]
20. Guo, L.; Hao, Y.W.; Li, P.L.; Song, J.F.; Yang, R.Z.; Fu, X.Y.; Xie, S.Y.; Zhao, J.; Zhang, Y.L. Improved NO₂ Gas Sensing Properties of Graphene Oxide Reduced by Two-beam-laser Interference. *Sci. Rep.* **2018**, *8*, 4918. [[CrossRef](#)] [[PubMed](#)]
21. Zhang, W.; Zhang, D.; Zhang, Y. High-performance NO₂ gas sensor based on bimetallic oxide CuWO₄ decorated with reduced graphene oxide. *J. Mater. Sci. Mater. Electron.* **2020**, *31*, 6706–6715. [[CrossRef](#)]
22. Lim, N.; Kim, H.; Pak, Y.; Byun, Y.T. Enhanced NO₂ sensing performance of graphene with thermally induced defects. *Materials* **2021**, *14*, 2347. [[CrossRef](#)] [[PubMed](#)]
23. Lee, J.S.; Kwon, O.S.; Shin, D.H.; Jang, J. WO₃ nanonodule-decorated hybrid carbon nanofibers for NO₂ gas sensor application. *J. Mater. Chem. A* **2013**, *1*, 9099–9106. [[CrossRef](#)]
24. Cha, J.-H.; Choi, S.-J.; Yu, S.; Kim, I.-D. 2D WS₂-edge functionalized multi-channel carbon nanofibers: Effect of WS₂ edge-abundant structure on room temperature NO₂ sensing. *J. Mater. Chem. A* **2017**, *5*, 8725–8732. [[CrossRef](#)]
25. Drewniak, S.; Drewniak, L.; Pustelny, T. Mechanisms of NO₂ Detection in Hybrid Structures Containing Reduced Graphene Oxide: A Review. *Sensors* **2022**, *22*, 5316. [[CrossRef](#)] [[PubMed](#)]
26. Han, T.H.; Huang, Y.-K.; Tan, A.T.L.; Dravid, V.P.; Huang, J. Steam Etched Porous Graphene Oxide Network for Chemical Sensing. *J. Am. Chem. Soc.* **2011**, *133*, 15264–15267. [[CrossRef](#)] [[PubMed](#)]
27. Lapekin, N.I.; Golovakhin, V.V.; Kim, E.Y.; Bannov, A.G. NO₂ Sensing Behavior of Compacted Chemically Treated Multi-Walled Carbon Nanotubes. *Micromachines* **2022**, *13*, 1495. [[CrossRef](#)] [[PubMed](#)]
28. Xu, Y.; Zhang, C.; Zhou, M.; Fu, Q.; Zhao, C.; Wu, M.; Lei, Y. Highly nitrogen doped carbon nanofibers with superior rate capability and cyclability for potassium ion batteries. *Nat. Commun.* **2018**, *9*, 1720. [[CrossRef](#)]
29. Bayat, N.; Rezaei, M.; Meshkani, F. CO_x-free hydrogen and carbon nanofibers production by methane decomposition over nickel-alumina catalysts. *Korean J. Chem. Eng.* **2016**, *33*, 490–499. [[CrossRef](#)]
30. Ermakova, M.A.; Ermakov, D.Y.; Chuvilin, A.L.; Kuvshinov, G.G. Decomposition of methane over iron catalysts at the range of moderate temperatures: The influence of structure of the catalytic systems and the reaction conditions on the yield of carbon and morphology of carbon filaments. *J. Catal.* **2001**, *201*, 183–197. [[CrossRef](#)]
31. Ermakova, M.A.; Ermakov, D.Y.; Kuvshinov, G.G. Effective catalysts for direct cracking of methane to produce hydrogen and filamentous carbon. Part I. Nickel catalysts. *Appl. Catal. A Gen.* **2000**, *201*, 61–70. [[CrossRef](#)]
32. Shinkarev, V.V.; Glushenkov, A.M.; Kuvshinov, D.G.; Kuvshinov, G.G. Nanofibrous carbon with herringbone structure as an effective catalyst of the H₂S selective oxidation. *Carbon N. Y.* **2010**, *48*, 2004–2012. [[CrossRef](#)]
33. Krutskii, Y.L.; Bannov, A.G.; Antonova, E.V.; Sokolov, V.V.; Pichugin, A.Y.; Maksimovskii, E.A.; Krutskaya, T.M.; Netskina, O.V.; Bataev, I.A. Synthesis of fine dispersed titanium diboride from nanofibrous carbon. *Ceram. Int.* **2017**, *43*, 3212–3217. [[CrossRef](#)]

34. Shestakov, V.A.; Gudyma, T.S.; Krutskii, Y.L.; Uvarov, N.F.; Brester, A.E.; Skovorodin, I.N. Evaluation of the Temperature Range Suitable for the Synthesis of B4C–TiB2 and B4C–ZrB2 Powder Composite Materials. *Inorg. Mater.* **2021**, *57*, 481–486. [CrossRef]
35. Krutskii, Y.L.; Gudyma, T.S.; Dyukova, K.D.; Kuz'min, R.I.; Krutskaya, T.M. Diborides of transition metals: Properties, application and production. Review. Part 2. Chromium and zirconium diborides. *Izv. Ferr. Metall.* **2021**, *64*, 395–412. [CrossRef]
36. Bannov, A.G.; Uvarov, N.F.; Shilovskaya, S.M.; Kuvshinov, G.G. Effect of the preparation methods on electrical properties of epoxy resin/carbon nanofiber composites. *Nanotechnol. Russ.* **2012**, *7*, 169–177. [CrossRef]
37. Brester, A.E.; Golovakhin, V.V.; Novgorodtseva, O.N.; Lapekin, N.I.; Shestakov, A.A.; Ukhina, A.V.; Prosanov, I.Y.; Maksimovskii, E.A.; Popov, M.V.; Bannov, A.G. Chemically Treated Carbon Nanofiber Materials for Supercapacitors. *Dokl. Chem.* **2021**, *501*, 264–269. [CrossRef]
38. Shinkarev, V.V.; Glushenkov, A.M.; Kuvshinov, D.G.; Kuvshinov, G.G. New effective catalysts based on mesoporous nanofibrous carbon for selective oxidation of hydrogen sulfide. *Appl. Catal. B Environ.* **2009**, *85*, 180–191. [CrossRef]
39. Kurmashov, P.B.; Bannov, A.G.; Popov, M.V.; Brester, A.E.; Ukhina, A.V.; Ishchenko, A.V.; Maksimovskii, E.A.; Tolstobrova, L.I.; Chulkov, A.O.; Kuvshinov, G.G. COx-free catalytic decomposition of methane over solution combustion synthesis derived catalyst: Synthesis of hydrogen and carbon nanofibers. *Int. J. Energy Res.* **2022**, 11957–11971. [CrossRef]
40. Yan, Q.; Ketelboeter, T.; Cai, Z. Production of COx-Free Hydrogen and Few-Layer Graphene Nanoplatelets by Catalytic Decomposition of Methane over Ni-Lignin-Derived Nanoparticles. *Molecules* **2022**, *27*, 503. [CrossRef]
41. Kuvshinov, D.G.; Kurmashov, P.B.; Bannov, A.G.; Popov, M.V.; Kuvshinov, G.G. Synthesis of Ni-based catalysts by hexamethylenetetramine-nitrates solution combustion method for co-production of hydrogen and nanofibrous carbon from methane. *Int. J. Hydrogen Energy* **2019**, *44*, 16271–16286. [CrossRef]
42. Shelepova, E.V.; Maksimova, T.A.; Bauman, Y.I.; Mishakov, I.V.; Vedyagin, A.A. Experimental and Simulation Study on Coproduction of Hydrogen and Carbon Nanomaterials by Catalytic Decomposition of Methane-Hydrogen Mixtures. *Hydrogen* **2022**, *3*, 450–462. [CrossRef]
43. Lumbers, B.; Agar, D.W.; Gebel, J.; Platte, F. Mathematical modelling and simulation of the thermo-catalytic decomposition of methane for economically improved hydrogen production. *Int. J. Hydrogen Energy* **2022**, *47*, 4265–4283. [CrossRef]
44. Lumbers, B.; Barley, J.; Platte, F. Low-emission hydrogen production via the thermo-catalytic decomposition of methane for the decarbonisation of iron ore mines in Western Australia. *Int. J. Hydrogen Energy* **2022**, *47*, 16347–16361. [CrossRef]
45. Kuvshinov, G.G.; Mogilykh, Y.I.; Kuvshinov, D.G. Kinetics of carbon formation from CH4-H2 mixtures over a nickel containing catalyst. *Catal. Today* **1998**, *42*, 357–360. [CrossRef]
46. Scherrer, P. *Bestimmung der inneren Struktur und der Größe von Kolloidteilchen mittels Röntgenstrahlen BT—Kolloidchemie Ein Lehrbuch*; Zsigmondy, R., Ed.; Springer: Berlin/Heidelberg, Germany, 1912; pp. 387–409. ISBN 978-3-662-33915-2.
47. Tuinstra, F.; Coenig, J. Characterization of graphite fiber surface with Raman spectroscopy. *J. Compos. Mater.* **1970**, *4*, 492–499. [CrossRef]
48. Kuvshinov, G.G.; Chukanov, I.S.; Krutsky, Y.L.; Ochkov, V.V.; Zaikovskii, V.I.; Kuvshinov, D.G. Changes in the properties of fibrous nanocarbons during high temperature heat treatment. *Carbon N. Y.* **2009**, *47*, 215–225. [CrossRef]
49. Bannov, A.G.; Uvarov, N.F.; Ukhina, A.V.; Chukanov, I.S.; Dyukova, K.D.D.; Kuvshinov, G.G. Structural changes in carbon nanofibers induced by ball milling. *Carbon N. Y.* **2012**, *50*, 1090–1098. [CrossRef]
50. Bannov, A.G.; Jašek, O.; Manakhov, A.; Márik, M.; Nečas, D.; Zajíčková, L. High-Performance Ammonia Gas Sensors Based on Plasma Treated Carbon Nanostructures. *IEEE Sens. J.* **2017**, *17*, 1964–1970. [CrossRef]
51. Ueda, T.; Bhuiyan, M.M.H.; Norimatsu, H.; Katsuki, S.; Ikegami, T.; Mitsugi, F. Development of carbon nanotube-based gas sensors for NOx gas detection working at low temperature. *Phys. E Low-Dimens. Syst. Nanostruct.* **2008**, *40*, 2272–2277. [CrossRef]
52. Zhang, Y.H.; Chen, Y.B.; Zhou, K.G.; Liu, C.H.; Zeng, J.; Zhang, H.L.; Peng, Y. Improving gas sensing properties of graphene by introducing dopants and defects: A first-principles study. *Nanotechnology* **2009**, *20*, 185504. [CrossRef]
53. Yan, W.; Worsley, M.A.; Pham, T.; Zettl, A.; Carraro, C.; Maboudian, R. Effects of ambient humidity and temperature on the NO2 sensing characteristics of WS2/graphene aerogel. *Appl. Surf. Sci.* **2018**, *450*, 372–379. [CrossRef]
54. Kim, C.H.; Yoo, S.W.; Nam, D.W.; Seo, S.; Lee, J.H. Effect of temperature and humidity on NO2 and NH3 gas sensitivity of bottom-gate graphene FETs prepared by ICP-CVD. *IEEE Electron. Device Lett.* **2012**, *33*, 1084–1086. [CrossRef]
55. Bannov, A.G.; Jašek, O.; Manakhov, A.; Márik, M.; Nečas, D.; Zajíčková, L.; Prášek, J.; Jašek, O.; Zajíčková, L. Investigation of pristine graphite oxide as room-temperature chemiresistive ammonia gas sensing material. *Sensors* **2017**, *17*, 320. [CrossRef]
56. Bannov, A.G.; Prášek, J.; Jašek, O.; Shibaev, A.A.; Zajíčková, L. Investigation of Ammonia Gas Sensing Properties of Graphite Oxide. *Procedia Eng.* **2016**, *168*, 231–234. [CrossRef]
57. Lee, M.J.; Yoo, K.; Min, N.; Park, C.; Kwon, K. Effects of various surface modifications on gas sensing characteristics of MWCNT/polyaniline composite films. pp. 1109–1112. Available online: <https://ieeexplore.ieee.org/document/5398570> (accessed on 9 December 2022).
58. Choi, S.W.; Kim, J.; Byun, Y.T. Highly sensitive and selective NO2 detection by Pt nanoparticles-decorated single-walled carbon nanotubes and the underlying sensing mechanism. *Sens. Actuators B Chem.* **2017**, *238*, 1032–1042. [CrossRef]
59. Yang, Z.; Zhang, D.; Chen, H. MOF-derived indium oxide hollow microtubes/MoS2 nanoparticles for NO2 gas sensing. *Sens. Actuators B Chem.* **2019**, *300*, 127037. [CrossRef]

60. Zhang, Y.; Jiang, Y.; Duan, Z.; Wu, Y.; Zhao, Q.; Liu, B.; Huang, Q.; Yuan, Z.; Li, X.; Tai, H. Edge-enriched MoS₂ nanosheets modified porous nanosheet-assembled hierarchical In₂O₃ microflowers for room temperature detection of NO₂ with ultrahigh sensitivity and selectivity. *J. Hazard. Mater.* **2022**, *434*, 128836. [[CrossRef](#)]
61. Peng, S.; Cho, K.; Qi, P.; Dai, H. Ab initio study of CNT NO₂ gas sensor. *Chem. Phys. Lett.* **2004**, *387*, 271–276. [[CrossRef](#)]
62. Mohammadi, M.; Ameri Shahrabi, M.J.; Sedighi, M. Comparative study of linearized and non-linearized modified Langmuir isotherm models on adsorption of asphaltene onto mineral surfaces. *Surf. Eng. Appl. Electrochem.* **2012**, *48*, 234–243. [[CrossRef](#)]
63. Katkov, M.V.; Sysoev, V.I.; Gusel, A.V.; Asanov, I.P.; Bulusheva, L.G.; Okotrub, A.V.; Gusel’Nikov, A.V.; Asanov, I.P.; Bulusheva, L.G.; Okotrub, A.V. A backside fluorine-functionalized graphene layer for ammonia detection. *Phys. Chem. Chem. Phys.* **2015**, *17*, 444–450. [[CrossRef](#)]
64. Fierro, V.; Schuurman, Y.; Mirodatos, C. *Simultaneous Determination of Intrinsic Adsorption and Diffusion of n-Butane in Activated Carbons by Using the TAP Reactor*; Elsevier B.V.: Amsterdam, Netherlands, 2007; Volume 160.
65. Hasanpour, M.; Hatami, M. Application of three dimensional porous aerogels as adsorbent for removal of heavy metal ions from water/wastewater: A review study. *Adv. Colloid Interface Sci.* **2020**, *284*, 102247. [[CrossRef](#)]
66. Salvestrini, S.; Ambrosone, L.; Kopinke, F.D. Some mistakes and misinterpretations in the analysis of thermodynamic adsorption data. *J. Mol. Liq.* **2022**, *352*, 118762. [[CrossRef](#)]
67. Liu, L.; Luo, X.B.; Ding, L.; Luo, S.L. *Application of Nanotechnology in the Removal of Heavy Metal from Water*; Elsevier Inc.: Amsterdam, Netherlands, 2018; ISBN 9780128148389.
68. Bo, S.; Ren, W.; Lei, C.; Xie, Y.; Cai, Y.; Wang, S.; Gao, J.; Ni, Q.; Yao, J. Flexible and porous cellulose aerogels/zeolitic imidazolate framework (ZIF-8) hybrids for adsorption removal of Cr(IV) from water. *J. Solid State Chem.* **2018**, *262*, 135–141. [[CrossRef](#)]
69. Zhou, Y.; Liang, C.Y.; Yu, J.G.; Jiang, X. Adsorption properties of a novel 3D graphene/MgO composite for heavy metal ions. *J. Cent. South Univ.* **2019**, *26*, 813–823. [[CrossRef](#)]
70. Hadian, M.; Marvee, D.P.F.; Buist, K.A.; Reesink, B.H.; Bos, A.N.R.; Van, A.P.B.; Kuipers, J.A.M. Kinetic study of thermocatalytic decomposition of methane over nickel supported catalyst in a fluidized bed reactor. *Chem. Eng. Sci.* **2022**, *260*, 117938. [[CrossRef](#)]
71. Navale, S.T.; Chougule, M.A.; Patil, V.B.; Mane, A.T. Highly sensitive, reproducible, selective and stable CSA-polypyrrole NO₂ sensor. *Synth. Met.* **2014**, *189*, 111–118. [[CrossRef](#)]
72. Chung, M.G.; Kim, D.H.; Lee, H.M.; Kim, T.; Choi, J.H.; Seo, D.K.; Yoo, J.-B.; Hong, S.-H.; Kang, T.J.; Kim, Y.H. Highly sensitive NO₂ gas sensor based on ozone treated graphene. *Sens. Actuators B Chem.* **2012**, *166–167*, 172–176. [[CrossRef](#)]
73. Sysoev, V.I.; Bulavskiy, M.O.; Pinakov, D.V.; Chekhova, G.N.; Asanov, I.P.; Gevko, P.N.; Bulusheva, L.G.; Okotrub, A.V. Chemiresistive Properties of Imprinted Fluorinated Graphene Films. *Materials* **2020**, *13*, 3538. [[CrossRef](#)]
74. Sysoev, V.I.; Okotrub, A.V.; Asanov, I.P.; Gevko, P.N.; Bulusheva, L.G. Advantage of graphene fluorination instead of oxygenation for restorable adsorption of gaseous ammonia and nitrogen dioxide. *Carbon N. Y.* **2017**, *118*, 225–232. [[CrossRef](#)]
75. Rattan, S.; Kumar, S.; Goswamy, J.K. Gold nanoparticle decorated graphene for efficient sensing of NO₂ gas. *Sens. Int.* **2022**, *3*, 100147. [[CrossRef](#)]
76. Liu, B.; Liu, X.; Yuan, Z.; Jiang, Y.; Su, Y.; Ma, J.; Tai, H. A flexible NO₂ gas sensor based on polypyrrole/nitrogen-doped multiwall carbon nanotube operating at room temperature. *Sens. Actuators B Chem.* **2019**, *295*, 86–92. [[CrossRef](#)]